AD-A273 544

NTATION PAGE

Form Approved
OMB No. 0704-0188

(2)

1. AGENCY USE ONLY (Leave blank)	2. REPORT DATE	3. REPORT TYPE AND DATES COVERED
	10/11/93	Final: Feb. 1990 - Jan. 1993

4. TITLE AND SUBTITLE
Interactive Control in Turbulent Shear Layers

5. FUNDING NUMBERS
2307/BS
G-AFOSR-90-0171

6. AUTHOR(S)
Candace E. Wark
Hassan M. Nagib

7. PERFORMING ORGANIZATION NAME(S) AND ADDRESS(ES)
Illinois Institute of Technology
Fluid Dynamics Research Center
10 West 32nd Street
Chicago, IL 60616

8. PERFORMING ORGANIZATION REPORT NUMBER

9. SPONSORING / MONITORING AGENCY NAME(S) AND ADDRESS(ES)
AFOSR/NA
Building 410
Bolling AFB DC 20332-6448
NA

10. SPONSORING / MONITORING AGENCY REPORT NUMBER
AFOSR-90-0171

11. SUPPLEMENTARY NOTES

12a. DISTRIBUTION / AVAILABILITY STATEMENT
Approved for Public Release; distribution is unlimited

12b. DISTRIBUTION CODE

13. ABSTRACT (Maximum 200 words)

Investigations of wall-bounded shear flow at IIT have been primarily focused on the following issues: i) inner- and outer-layer effects on the dynamics of a turbulent boundary layer (TBL), ii) a PIV study of fully developed turbulent pipe flow, iii) the effects of intermittency on the wall-layer dynamics and iv) the visualization of active events near the wall. The motivations behind these investigations are to understand the Reynolds number sensitivity and relative importance of the different scales of motion, with regard to the dynamics of turbulent wall-bounded flow and to document and study the *instantaneous* structure of the flow vis-a-vis the numerous coherent structure studies of the last two decades. A temporal filtering scheme was devised to separate the contribution of the different scales of motion to the u' signal and the Reynolds stress in the buffer and logarithmic region. Also, using PIV, instantaneous large-scale structures were observed, which are not seen in low Reynolds number direct numerical simulations of bounded turbulent shear flows. The analysis of flow visualization records of active events in a TBL was performed in the frame of a conjectured model that is based on Theodorsen's original hairpin vortex flow module. Information on the character, size, location, intensity and duration of the events was documented and tabulated.

14. SUBJECT TERMS	15. NUMBER OF PAGES
Reynolds Number Scaling Turbulent Boundary Layers	25
	16. PRICE CODE

17. SECURITY CLASSIFICATION OF REPORT	18. SECURITY CLASSIFICATION OF THIS PAGE	19. SECURITY CLASSIFICATION OF ABSTRACT	20. LIMITATION OF ABSTRACT
Unclassified	Unclassified	Unclassified	UL

INTERACTIVE CONTROL IN TURBULENT SHEAR LAYERS

FINAL TECHNICAL REPORT

AFOSR-90-0171

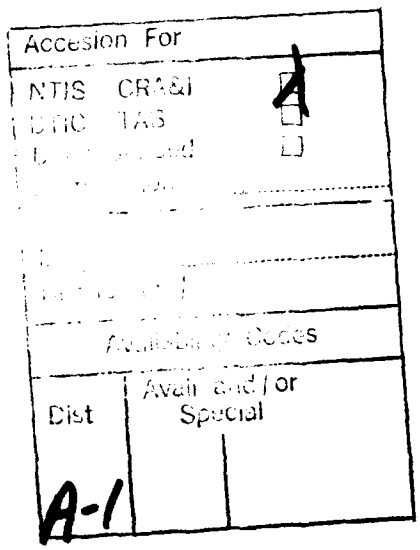

INVESTIGATORS:

Candace E. Wark
Hassan M. Nagib

February 1990 - January 1993

ILLINOIS INSTITUTE OF TECHNOLOGY

Fluid Dynamics Research Center
&
Mechanical and Aerospace Engineering Department

Chicago, Illinois 60616

Table of Contents

INTERACTIVE CONTROL IN TURBULENT SHEAR LAYERS

Introduction

Investigations of wall-bounded shear flows at IIT have been primarily focused on the following issues: i) inner- and outer-layer effects on the dynamics of a turbulent boundary layer, ii) a PIV study of fully-developed turbulent pipe flow, iii) the effects of intermittency on the wall-layer dynamics and iv) the visualization of active events near the wall. The motivations behind these investigations are to understand the Reynolds number sensitivity and relative importance of the different scales of motion, with regard to the dynamics of turbulent wall-bounded flows and to document and study the *instantaneous* structure of the flow vis-a-vis the numerous coherent structure studies of the last two decades.

An Investigation of Wall-Layer Dynamics Using a Combined Temporal Filtering and Correlation Technique

Inner- and Outer-Layer Effects on the Dynamics of a Turbulent Boundary Layer

In the first investigation, a temporal filtering scheme was devised to separate the contribution of the different scales of motion to the u' signal and the Reynolds stress in the buffer and logarithmic regions. The scaling characteristics of the power spectra ($\phi_{u'u'}(f)$) were used to choose the cut-off frequencies for the temporal filters. As an example, the power spectra for $y^+ = 50$ and 100 are given in the top of Figure 1. Wall-scaling was found to collapse the spectra successfully for all Reynolds numbers, provided the frequency is larger than $f^+ \cong 0.003$. The Reynolds number effect at low frequencies in the logarithmic region has also been documented in the spectra measured by Perry and Abell (1977) and more recently by Antonia et al. (1992). The bottom plots in Figure 1 represent the results for the spectra normalized by outer variables at $y/\theta = 0.445$ and 1.0 in the logarithmic region. Except for $Re_\theta < 3000$ at $y/\theta = 0.445$, no significant viscous effects are observed and the spectra collapse very well with the outer length scale for all frequencies.

It is straightforward to show that if a quantity scales with θ and ν/u_τ simultaneously it will also collapse with y. Thus, the results in Figure 1 also indicate that the spectra in the logarithmic region will collapse for $f^+ > 0.003$ when using y as the length scale in normalizing the spectra. This agrees with the ideas of Perry and Abel (1977) on universal scaling of the function $\phi_{u'u'}(fy/U)$ for the energy containing eddies in the logarithmic region.

Perry, Henbest and Chong (1986) (hereafter referred to as PHC) suggested that the moderate- to high-wave-number u' velocity fluctuations are generated by turbulent motion whose size is approximately equal to the local height y. Thus, they anticipated $\phi_{u'u'}$ to *scale* with y for the intermediate wave-number range. Furthermore PHC expected the resulting *collapse* of $\phi_{u'u'}$ on y to be valid *down* to wavenumbers where k_x becomes sufficiently small such that it corresponds to eddies whose size is of order δ. This should happen at a wavenumber given by $k_x\delta = A$ ($f = AU/\delta$) where A is a constant of order

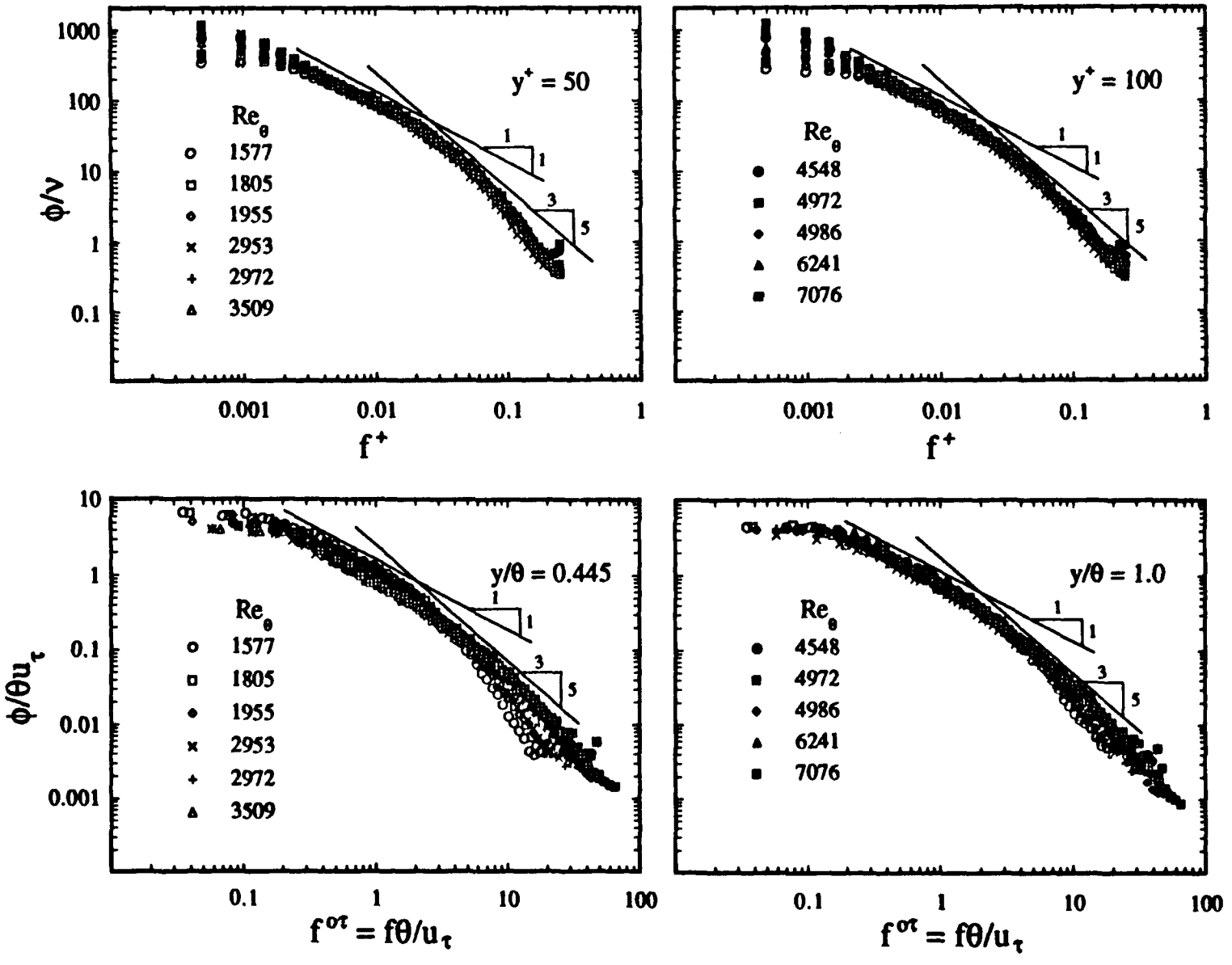

Figure 1. Wall Scaling (top) and Outer Scaling (bottom) characteristics of the Power Spectra in the Logarithmic Region at $y^+ = 50$ and $y^+ = 100$.

unity. According to the dimensional arguments of PHC, all frequencies below $f^+ = AU^+/\delta^+$ are generated by structures whose size is of order δ. Thus, a low-pass filter with a cut-off frequency $f^+_c = AU^+/\delta^+$ is expected to isolate the u' signature of *outer*-layer structures in the *logarithmic* region. Such a filter will be referred to as filter *lp,o*.

The cut-off frequency of filter *lp,o* when normalized with *outer* variables remains constant with changing Reynolds number. This may be seen by observing that the spectra in the top plots of Figure 1 follow the inverse power law form (as seen from the straight line with slope of -1) prior to departing from *inner collapse*. However, this departure is the same in *outer* variables for all Reynolds numbers (as seen from the bottom plots in Figure 1) and is approximately equal to 0.2 for $y/\theta = 0.445$ and 1.0. Thus, an alternative way of defining the cut-off frequency of filter *lp,o* is as the lower frequency limit of the inverse power law part of the spectra.

The range of wavenumbers (frequencies) where $\phi_{u'u'}$ follows the inverse power law represents an *overlap* region between structures of size of order δ and eddies of size of order y. This has been shown by PHC who demonstrated that the inverse power law is a dimensional necessity for the spectra in such an *overlap* region. Within this region, the spectra *collapse* with both θ and y, as may be verified from Figure 1. The *overlap* width, in wall units, increases with increasing Reynolds number as a result of the lower frequency limit of the *overlap* region shifting to lower f^+ values at higher Reynolds numbers. On the other hand, for a given y/θ location, the frequency range over which the *overlap* region is observed remains unchanged when f is normalized using *outer* variables.

The high-frequency end of the *overlap* region may be determined as the frequency above which the spectra deviate from the inverse power law behavior. At this frequency ($f^+ = BU^+/y^+$, B is a constant of order unity) the structures size becomes small enough to be of order y. Consequently, if a high-pass *temporal* filter is designed with its cut-off frequency set at that particular value, it should contain frequencies generated by structures of size of order y and smaller. Such a filter has been implemented to obtain the u' signature generated by the *inner*-layer turbulent motion in the *log* region and it will be denoted by filter *hp,y*. It should be noted here that without an explicit statement about the inverse-power-law behavior of the spectra in the *overlap* region, it would have not been possible to distinguish the region of the *overlap* from that where *y scaling* (order-y size structures) is observed.

It should also be added here, that the frequencies passed by filter *hp,y* contains not only motion which *scales* on y (i.e., *inner*) but also dissipative motion which *scales* with ν/u_τ with an inertial sub-range (-5/3 slope) filling the range of scales between y and ν/u_τ. No filters were designed to separate y- and ν/u_τ-size motions, since our main goal is to decompose the u' signature into *inner* and *outer* components only.

To estimate the energy for a given type of motion we simply filter the u' signal with the appropriate filter, followed by calculating the energy for the filtered time series. The percentage of the total u' energy and $\overline{u'v'}$ generated by the *inner*, *outer* and *overlap* turbulent motions is plotted in Figure 2 as a function of Re_θ. In each plot the full length of the vertical axis represents 100% of the local energy $(u'_{rms})^2$, or $\overline{u'v'}$ and the two curves shown by broken lines are curve fits to the data points. The distance between the bottom of the vertical axis to the lower curve is the percentage generated by the *outer*-layer, and

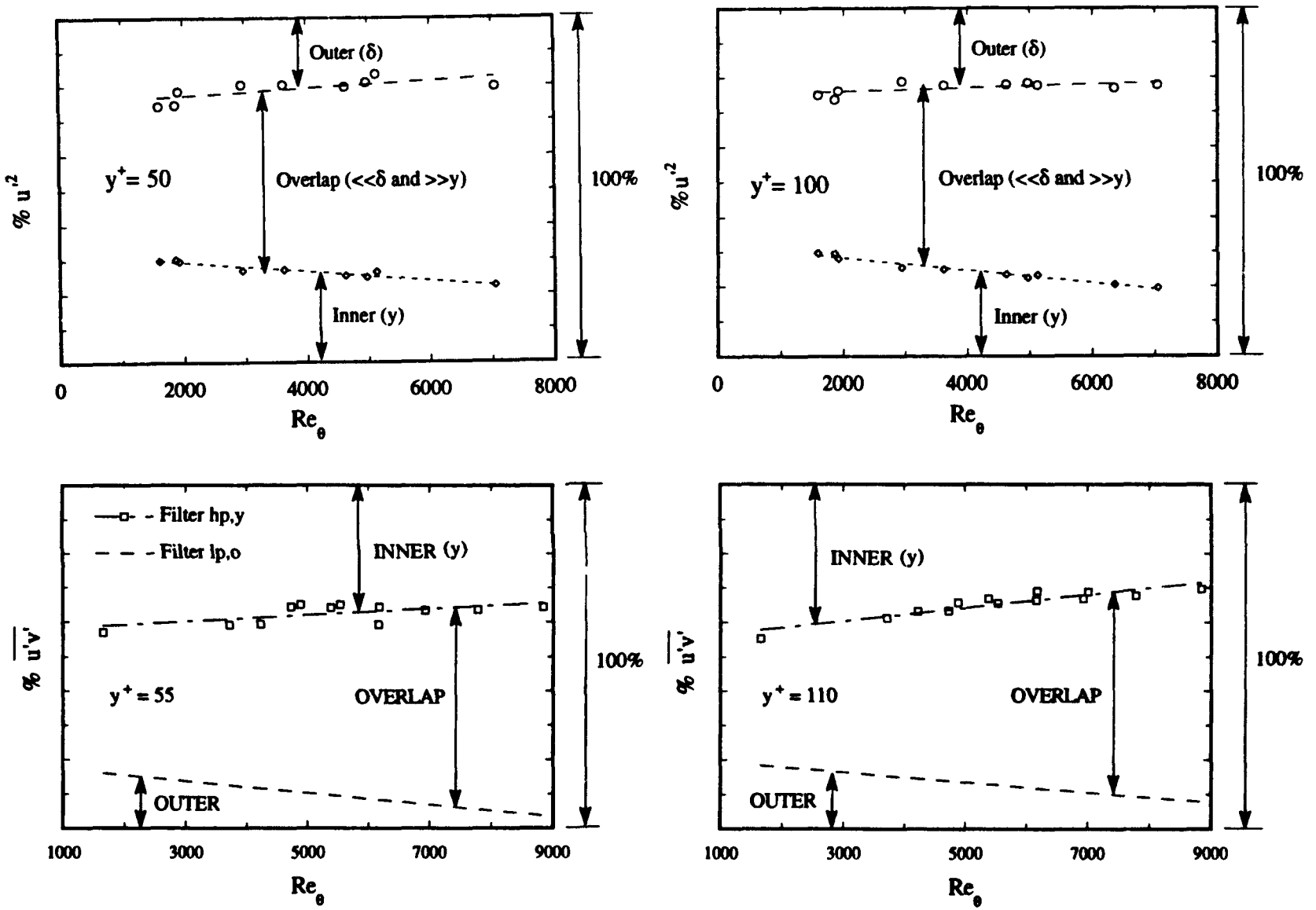

Figure 2. Relative Contribution of Inner, Overlap and Outer Turbulent Motion to the Streamwise Turbulent Kinetic Energy and Reynolds Stress Production in the Logarithmic region.

the distance between the upper curve to the top of the vertical axis is the percentage due to *inner*-layer eddies.

As seen from Figure 2, turbulent motion within the *overlap* region dominates the Reynolds stress production and streamwise turbulent kinetic energy. A considerable amount of $(u'_{rms})^2$, and $\overline{u'v'}$ is attributable to the *inner* layer. This contribution, however, decreases slowly with increasing Reynolds number at the expense of increased production by eddies within the *overlap* region. The *outer*-layer contribution to $\overline{u'v'}$ is approximately 19% at the lowest Reynolds number and it decreases monotonically to reach a value of about 5% at $Re_\theta = 8842$.

Structure of Turbulence Using PIV in a Wall-Bounded Shear Flow

Objective. The objective of this investigation is to document the instantaneous state of the turbulent flow and to i) compare this with the conditionally-averaged flowfield documented by various investigators over the last several decades and ii) decompose the spatial field into the contributions due to the outer, inner and overlap motions.

Experimental Procedure. A fully-developed turbulent pipe flow in air at Re_D= 50,000 was investigated using PIV. This work was the result of a collaboration between IIT and Professor Ron Adrian and Peter Offutt at the University of Illinois. The laser system consisted of a pair of Nd-YAG lasers with approximately 60 mJ of energy per pulse. Each laser was pulsed at 50 Hz, with a 46 μsec time delay between the two pulse trains. The photographs were double exposed and recorded using a 4 by 5 view camera. The flow was seeded with atomized olive-oil droplets approximately 1 to 5 μm in diameter. The data were taken in the x-y plane and each instantaneous realization spans approximately 2000 wall units in the streamwise direction and extends from $6 \leq y^+ \leq 700$ (the centerline of the pipe corresponds to $y^+ = 1300$). 120 photographs have been interrogated with each photograph yielding velocity measurements at more than 10,000 points.

Results. A filtering scheme, similar to that described above is being used to identify the instantaneous structures associated with the inner, outer and overlap turbulent motion. An example of this is given in Figure 3. The top plot in Figure 3 represents the unfiltered fluctuating velocity vectors resulting from one of the PIV photographs. The line-averaged profile was determined using all 120 photographs and matches very well with the time-averaged mean velocity profile resulting from a hot-wire survey. The line-averaged profile was subtracted from the results for each photograph yielding the fluctuating vector field. After filtering this fluctuating vector field using a high-pass and low-pass filter the middle and bottom plot, respectively, in Figure 3 results. To document the Reynolds number influence, a related investigation is being performed using PIV in a turbulent boundary layer over a range of Reynolds number from $2000 < Re_\theta < 10{,}000$.

Many previous investigations have documented conditionally-averaged large-scale structures (Guezennec 1985 and Wark and Nagib 1991). One question that remained unanswered however, was whether these large-scale structures actually exist in the flow or are they an artifact of the ensemble-averaging process. When viewing the velocity fields from the 120 realizations, it is evident that instantaneous "large-scale" structures occur

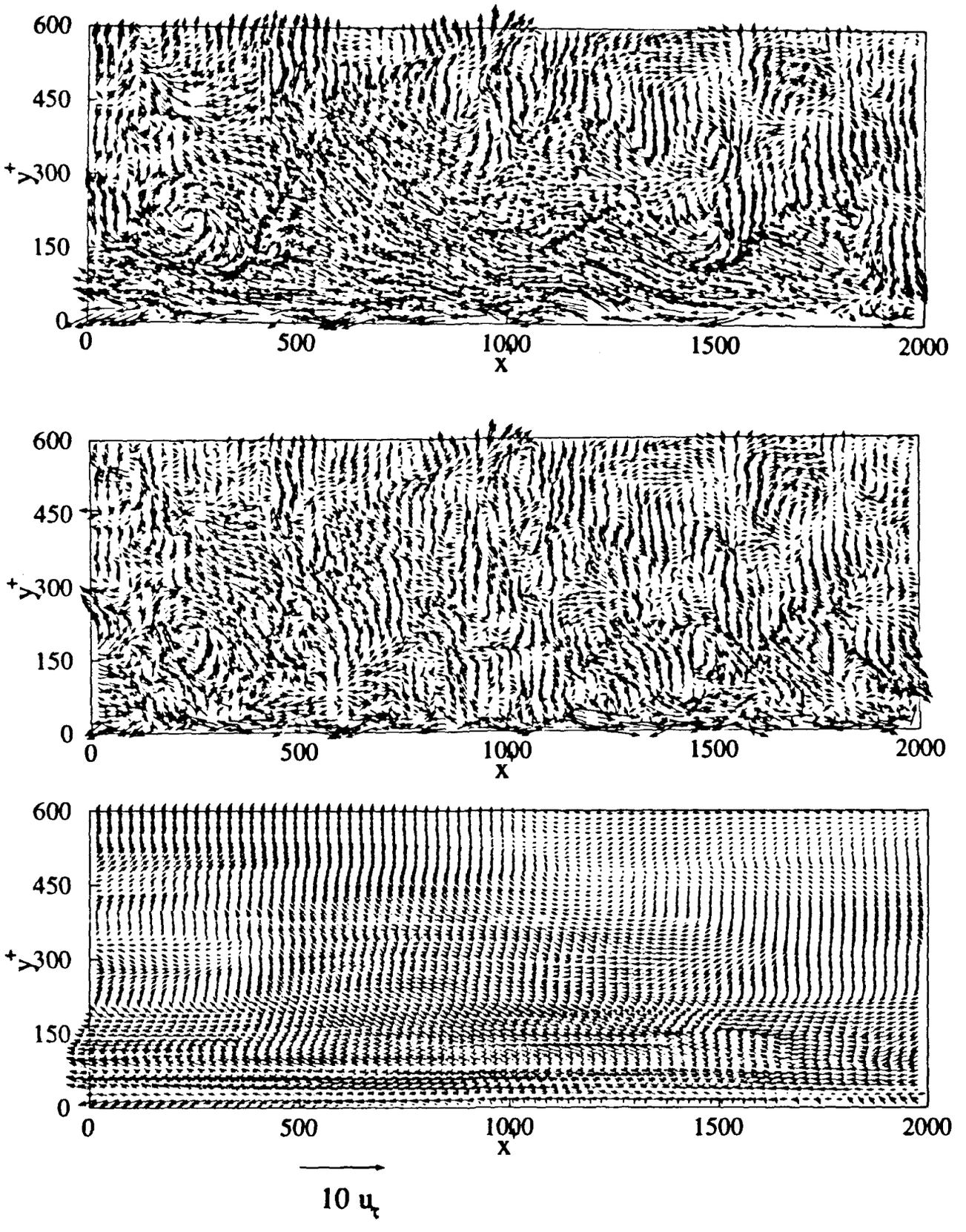

Figure 3. Velocity-Vector Map in a Fully-Developed Turbulent Pipe Flow for the Fluctuating Velocity Field (top plot), the result after filtering using a High-Pass (middle) and Low-Pass (bottom) filter.

very frequently (> 30%). The top plot in Figure 3 illustrates this point. A "large-scale" structure is evident for a spanwise duration of $x^+ \approx 1500$ and extends up to a $y^+ \approx 450$. This figure represents a "large-scale" "low-speed" region and one can easily see how this structure would contribute to the quadrant two (Q2) events. Likewise, there are also "large-scale" "high-speed" regions which would contribute to Q4 events in several of the 120 photographs. At present, the contribution of these structures to the Reynolds-stress production is being investigated.

Effects of Outer-Layer Intermittency on the Reynolds-Stress Producing Events in a Turbulent Boundary Layer

Objectives. The present study was conducted to determine the relation between the outer-layer intermittency and the wall layer turbulent production process. This investigation was performed in a zero pressure gradient turbulent boundary layer at Re_θ= 4942.

Experimental Procedure. Data was acquired with a X-wire probe which was traversed at various heights (y/δ = 0.4 to 1.5 in steps of 0.1) to detect the interface between turbulent and non-turbulent fluid, while a shear-wire probe was kept at $y^+ = 0$, and a single-wire was placed at one of four y^+ positions (y^+ = 10, 15, 30 and 55). The three probes were placed at the same streamwise location and the X-wire intermittency probe was placed at both $\Delta z^+ = 0$ and $\Delta z^+ = 80$ with respect to the single u-wire and shear-wire probes.

Results. Various statistical measures on the time series acquired by the shear-wire and single u-wire probes were determined when the X-wire intermittency detector probe encountered either turbulent or non-turbulent fluid. Conditional averages and probability density functions of the streamwise component of the wall shear-stress and streamwise velocity fluctuation normalized by their root mean square values (u/u_{rms} and τ/τ_{rms}) were obtained. Furthermore, the conditional U-level and shear-stress detected events were obtained to examine the effect of the outer-layer intermittency on the wall-layer turbulence production process.

The intermittency detector scheme employed in the present investigation is given by Hedley and Keffer (1974): this scheme is based on both the streamwise and normal components of velocity. A criterion function, $S(t_j)$, given by

$$S(t_j) = \frac{\Delta T^2}{1 + \frac{T_s}{\Delta T}} \sum_{i=j-\frac{T_s}{2\Delta T}}^{i=j+\frac{T_s}{2\Delta T}} \left\{ \left(\frac{Du}{DT}\right)^2 + \left(\frac{Dv}{DT}\right)^2 \right\}_i$$

was used to detect the turbulent/non-turbulent interface: ΔT is equal to 1/(acquisition frequency) and is 1.5e-04 sec and a non-dimensional hold time, $T_s/2\Delta T$, equal to two was used in this investigation.

An adjustable threshold level C equal to 0.1 was chosen to threshold the criterion function (S) such that the intermittency level at 0.8 y/δ was approximately 50%. This value of 50% for 0.8 y/δ is taken from the discussion of Kovasznay et al. (1970) and Corrsin and Kistler (1955). The resulting function is called an indicator or intermittency

function which is a random square wave with values of unity for turbulence and zero otherwise. This function was subsequently used to condition the signals from the single and shear-wire probes to study the effect of the outer-layer intermittency on wall-layer Reynolds-stress producing events.

The intermittency factor γ or $\overline{I}$ is then defined as the time-averaged value of the intermittency function $I(t_j)$: $\gamma = \overline{I} = \sum_{i=1}^{N} \frac{I(t_i)}{N}$ where N is the number of points in the time series.

The variation of the intermittency factor (γ) across the boundary layer varies smoothly from values of unity deep in the boundary layer to zero outside of the boundary layer. The profile matches the results by Kovasznay et al. (1970), Hedley and Keffer (1974) and Guezennec and Nagib (1990).

If we let $Q(t_j)$ represent an arbitrary time series, the *conventional* and *conditional* time average of $Q(t_j)$ when the intermittency detector has a value of one (often called a turbulent bulge) and zero (non-turbulent conditions) is given by:

$$\overline{Q} = \sum_{j=1}^{N} \frac{Q(t_j)}{N} \qquad Q_1 = \sum_{j=1}^{N} \left(\frac{I(t_j)Q(t_j)}{N\overline{I}} \right) \qquad Q_0 = \sum_{j=1}^{N} \left(\frac{[1-I(t_j)]Q(t_j)}{N[1-\overline{I}]} \right)$$

respectively. It then follows that $\overline{Q} = \gamma Q_0 + (1-\gamma)Q_1$.

The conditional probability distributions of u/u_{rms} are shown in Figure 4. The top plot represents the turbulent conditional zone average; whereas, the non-turbulent conditional zone average is given in the bottom plot. Only results for u/u_{rms} at $y^+=10$ are shown here: the results for τ/τ_{rms} and for u/u_{rms} at $y^+=15$, 30 and 50 are similar to those for $y^+=10$. The streamwise and spanwise offsets between the intermittency detector probe and streamwise velocity probe was $x^+=0$ and $z^+=0$ as given in the plots.

Blackwelder and Kovasznay (1972) obtained point averages of the streamwise velocity component as a function of the distance from the intermittency detector probe. The point averages of the streamwise velocity fluctuations at the "fronts" and "backs" of the turbulent bulge were found to be significantly different. The "front" of a turbulent bulge is defined as the location at which the probe detects a non-turbulent/turbulent interface; likewise, the "back" is the location where the probe detects a turbulent/non-turbulent interface. Based upon their results the present data was processed to determine the conditional zone averages upon detection of the "fronts" and "backs" of the turbulent bulges. Figure 5 depicts the conditional averages for u/u_{rms}. The conditional averages for the "fronts" and the "backs" are seen in the top and bottom plots respectively.

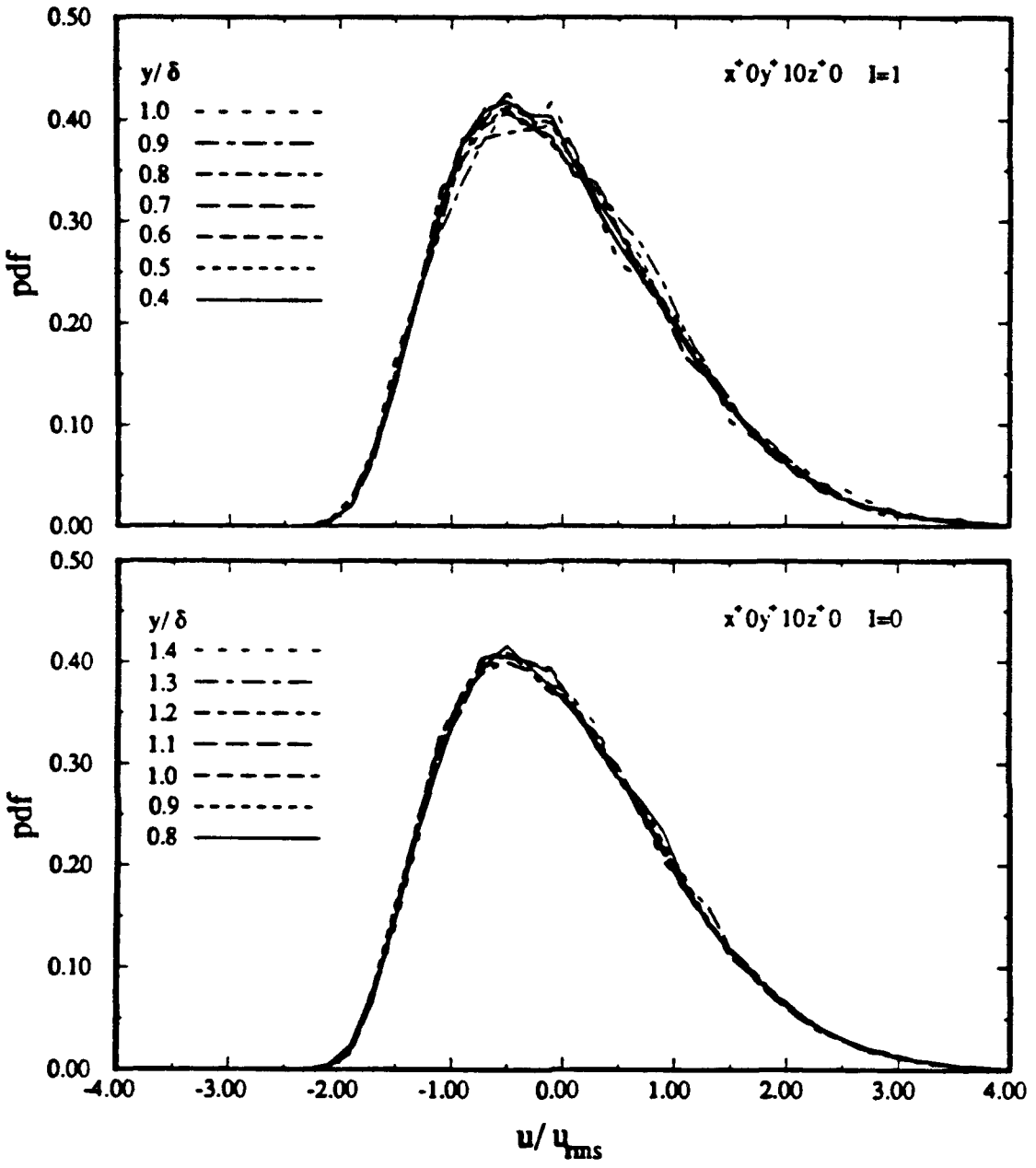

Figure 4. Comparison of Conditional Probability Density Functions of u/u_{rms} at $y^+= 10$, for I = 1 and 0, at several y/δ Intermittency Detector Positions.

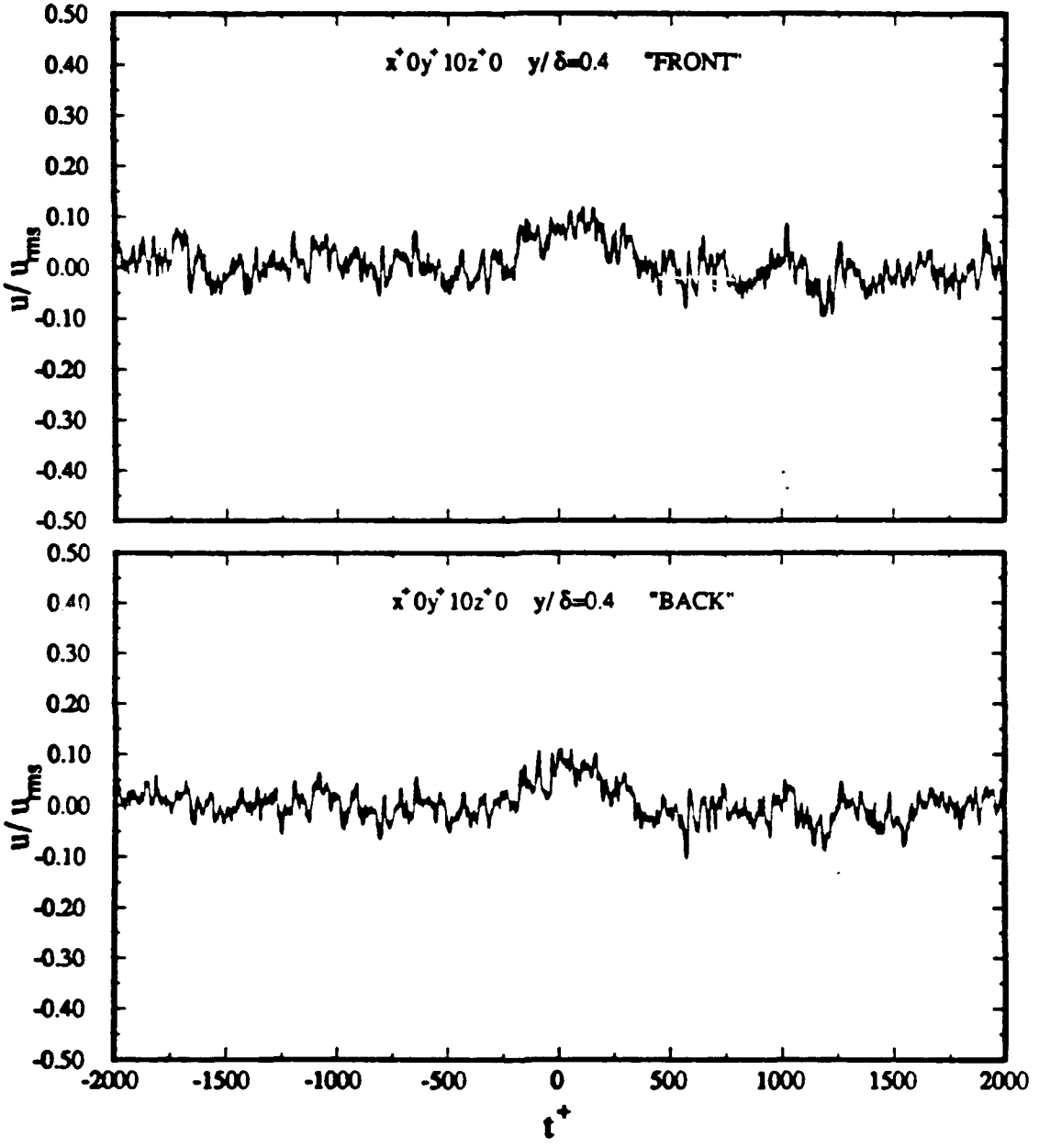

Figure 5. Comparison of Conditional Zone Averages of u/u_{rms} at $y^+= 10$, for the "fronts" and "backs" of Turbulent Bulges, as a function of t^+ for several y/δ Intermittency Detector Positions.

In addition, further processing to determine what effect, if any, the turbulent bulges have upon the Reynolds-stress producing events as detected by the U-level detection scheme from Lu and Willmarth (1973). The U-level detected events were counted either when the intermittency function (I) indicated turbulent or non-turbulent fluid. Normalized by the time duration of the turbulent bulge (T_v) or non-turbulent regions (T_{1-v}) for the two conditions I=1 and 0 respectively, the number of U-level detected events can be seen in Figure 6.

Concluding Remarks. Even though the influence of the outer-layer on the wall-layer has been documented, the results presented above suggest that the intermittent character of the outer flow in a turbulent boundary layer is not responsible for this influence. This is consistent with turbulent channel and pipe flow studies in the sense that the wall-layer statistics are remarkably similar between these three turbulent wall-bounded shear flows; yet, turbulent channel and pipe flow do not exhibit the same intermittent character as a turbulent boundary layer.

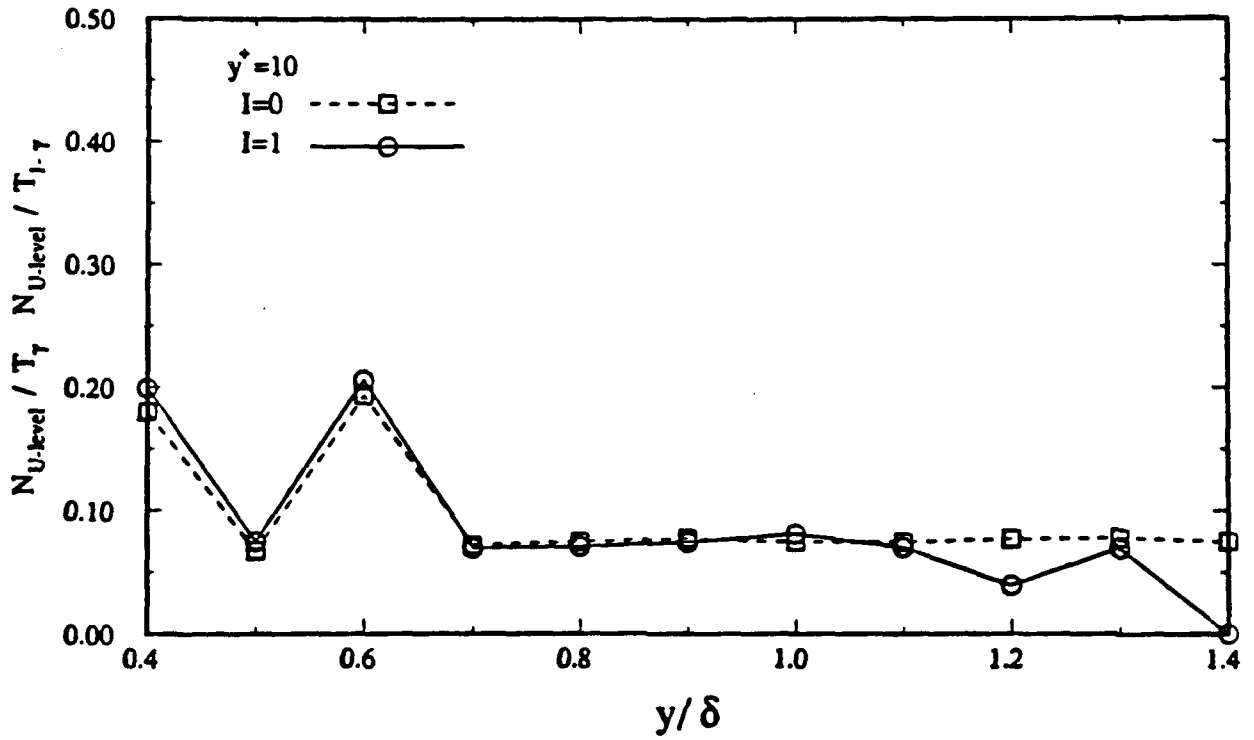

Figure 6. Comparison of Number of U-level Detected Events at $y^+ = 10$, for I = 1 and 0 as a function of Intermittency Detector Location.

Visualization of Dynamically Active Events in a Turbulent Boundary Layer

Summary. Two- and three-dimensional views of the turbulence in the wall region of a turbulent boundary layer were recorded on high speed film with the aid of locally introduced multiple smoke sheets and several laser-light planes. The simultaneous acquisition of the wall-shear signal at an Re_θ of 2100 allowed the identification and analysis of the instantaneous coherent structures associated with turbulence production. Information on the character, size, location, intensity and duration of these structures was cataloged and in most cases statistics were derived from them. The analysis of the visual records was carried out in the frame of a conjectured model which is based on extensions of Theodorsen's (1952) original hairpin vortex flow module.

Objectives. The focus of the present investigation is also to reveal the instantaneous dynamics of these structures by using flow visualization combined with a non-obtrusive detection probe (Guezennec, 1985) to identify and characterize the individual turbulence producing events. To aid in deciphering the films, a model, based on the hairpin vortex, is conjectured to be the dominant structure responsible for turbulence production in the boundary layer. Various two and three dimensional views of the visualizations are examined to find evidence that is in support of the model; see Figures 7 and 8.

Evidence of the Hairpin Vortex Structure. Several investigators have proposed the hairpin vortex as the basic flow module responsible for the production of the turbulent kinetic energy, and for sustaining the turbulence, in boundary layer flows. By pumping low momentum fluid up away from the wall in the middle (Q2 or ejection event), and pushing high momentum fluid down toward the wall on the sides (Q4 or sweep event), the hairpin vortex is generating the cross-gradient mixing necessary for the production of turbulent kinetic energy.

Many investigators have isolated components of the hairpin vortex, such as the streamwise vortices or the spanwise vortices forming the head, and have conjectured as to their relation with the hairpin vortex, but have failed to provide substantial evidence linking all of the hairpin vortex components together in a fully turbulent boundary layer. Using simultaneous views of the of the x-y and y-z planes in the Bi-Plane set up, Figure 8, it was hoped that the connection between the transverse vortices, seen as the curling over of ejected spindles of smoke, and the lifted streamwise vortices, seen as mushroom shapes in the spanwise view, would become apparent. However, due to the scarcity of smoke in the higher regions, and the difficulty in marking only the hairpin vortex element, this connection was never consistently made. It was noted that when fluid was violently ejected from the wall that large bulges of smoke appeared in the x-y plane after the ejection passed through. This could indicate the presence of the counter rotating legs of the hairpin vortex, pushing the smoke up in the middle.

The analysis of the high-speed visualization records, in connection with the wall-shear signals, revealed several cases after a T- detection with an arch-like structure appearing in the y-z plane centered about the plane of detection. In the case of T+ detection, the arch-like structure appeared to one side or on both sides of the central plane. However, due to the difficulty in examining the patterns in the y-z plane of the Bi-Plane configuration, the spanwise details of the bulges were unclear.

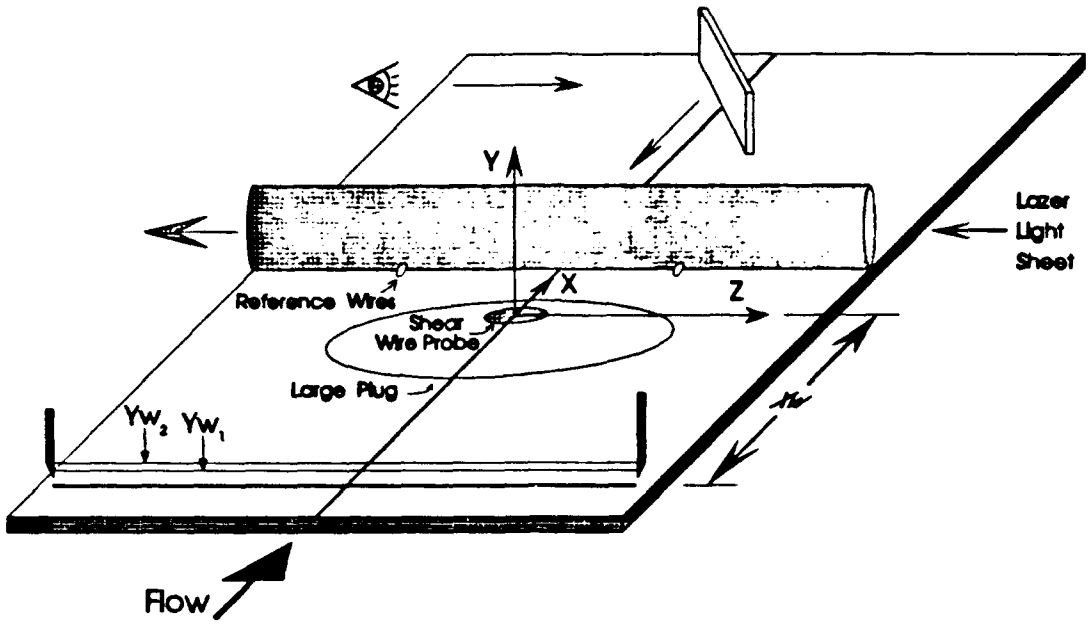

Figure 7a. Schematic of Laser-Light Sheets Arrangement for Z-Type Visualization Set Up.

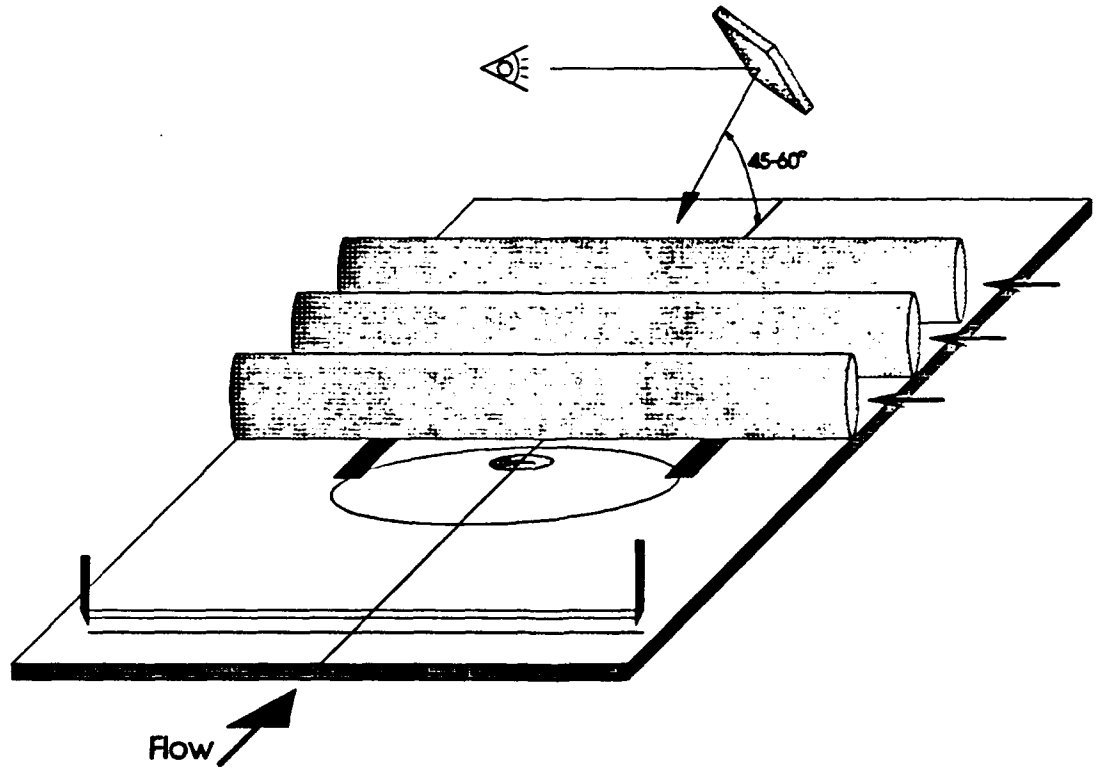

Figure 7b. Schematic of Laser-Light Sheets Arrangement for 3Z-Type Visualization Set Up.

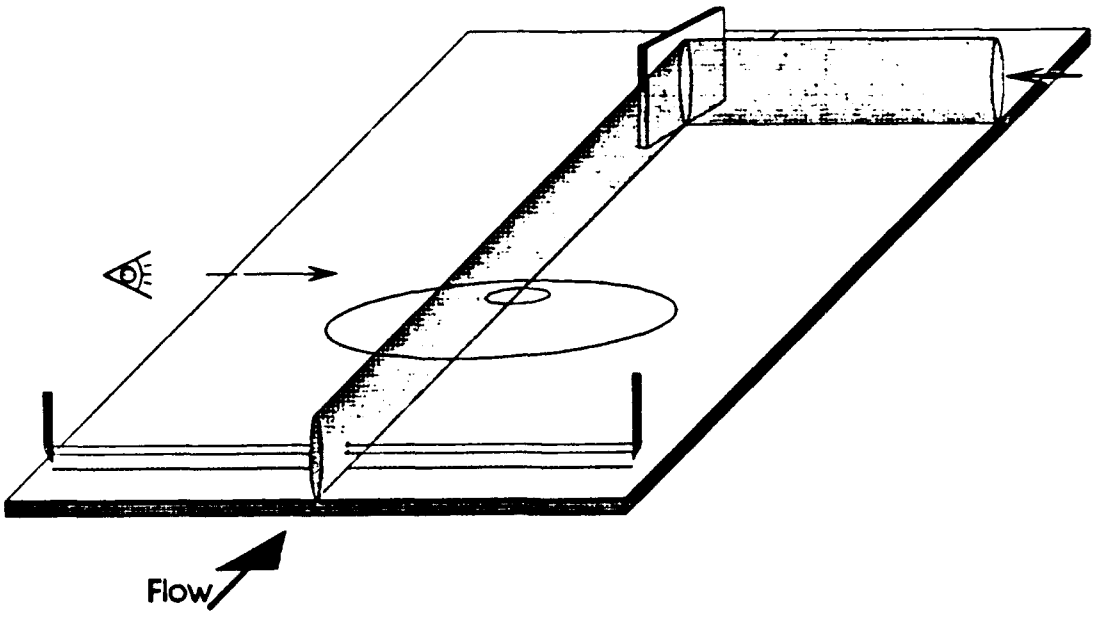

Figure 8a. Schematic of Lser-Light Sheets Arrangement for X-Type Visualization Set Up.

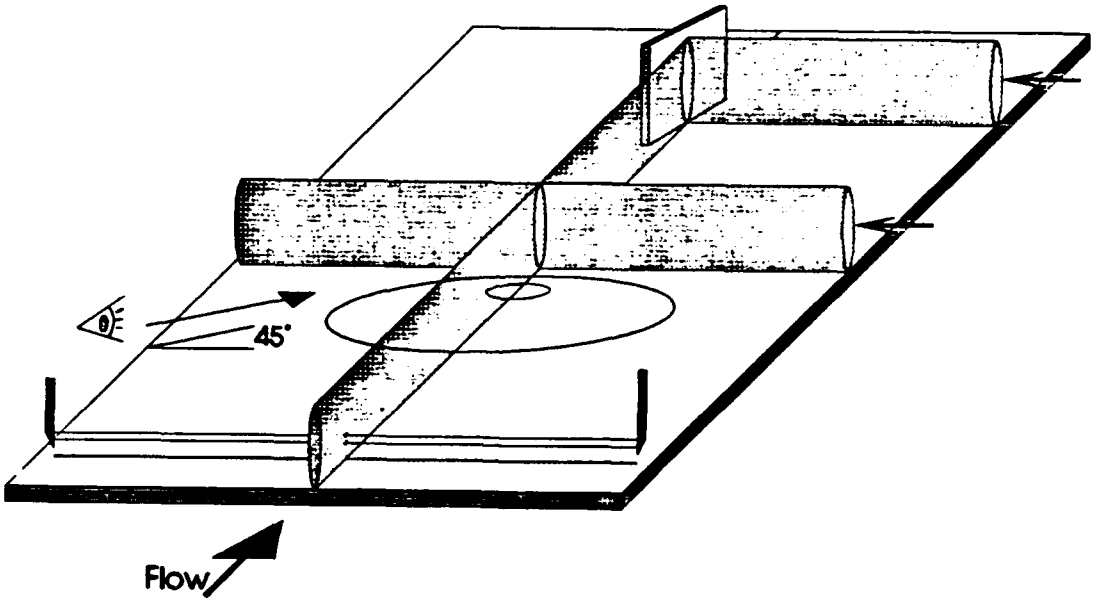

Figure 8b. Schematic of Laser-Light Sheets Arrangement for Bi-Plane Visualization Set Up.

More detailed information on the streamwise vortices was found in the Z-Type and 3Z-Type films, recorded using the arrangements of Figure 7. In both of these film types, a variety of mushroom shapes and question mark-like shapes appeared very often, signifying streamwise vortices. The 3Z-Type films also allowed for the investigation of the evolution of the structures as they passed through successive light sheets. Several progressions of structures passing through the sheets were traced onto grids. These tracings presented clear evidence of streamwise circulation between planes due to counter rotating vortices.

To further test the relation of the structures to T+ and T- events, the structures appearing in the Z-Type films were correlated with the shear-stress events. The correlation results indicate that T+ detections are associated with structures occurring farther away from the detection point. This is in support of the model since T- events should correspond to structures going over the top of the probe while T+ events should correspond to structures passing to the side of the probe. The results also indicate that the average spacing between successive structures occurring about the probe is larger for T+ associated structures than otherwise. This may indicate that the structures causing the strong T+ events are larger as they occur at larger spanwise spacings.

In summary, structures associated with the production of turbulence were found to have characteristics consistent with the hairpin vortex model. However, no consistent evidence is available of the fact that the streamwise and transverse vortices have to be a part of the same structure (the hairpin vortex) responsible for the production. Furthermore, a correlation was found between T+ events and structures occurring at larger spacings farther away from the detection probe, which is supportive of the model.

Spanwise Occurrence of Dynamically Active Events. Several probe based detection techniques were also developed to identify a burst, and were used to find the characteristics of the bursts, such as the bursting frequency, the conditionally averaged flow field associated with a burst, and so on. Other investigations dealing with the bursting event reveal information on the characteristics of single burst events, their relation to sweep events, or their rate of occurrence at a single streamwise station. None of these investigations deal with the relative spanwise occurrence or separation between these burst events. Similar observations can be made about the documentation of any of the features associated with strong production of Reynolds stresses in wall bounded flows.

In this investigation a technique has been developed which addresses the question of spanwise spacing and interaction between successive spanwise turbulence producing events and structures. The technique basically involves introducing smoke into the flow, using smoke wires parallel and near to the floor, and looking for vertical excursions of the smoke illuminated by a laser-light sheet oriented in the y-z plane and located 1100 x^+ downstream from the smoke wires. The vertical excursions of smoke seen in the films are referred to as ejection type structures whose strength is based on what threshold height they reach in the images; see Figure 9. The spanwise locations of such events are recorded for every forth frame in a high speed film. From these data the spacings between the structures as well as the structures duration in time can be investigated.

For this procedure the Z-Type film set up is used and both plain and artificially disturbed cases were examined. Some of the films had a high smoke wire configuration, where both sweep and ejection events could be identified. By following the structures from frame to frame, it became evident that some structures lasted for significant periods

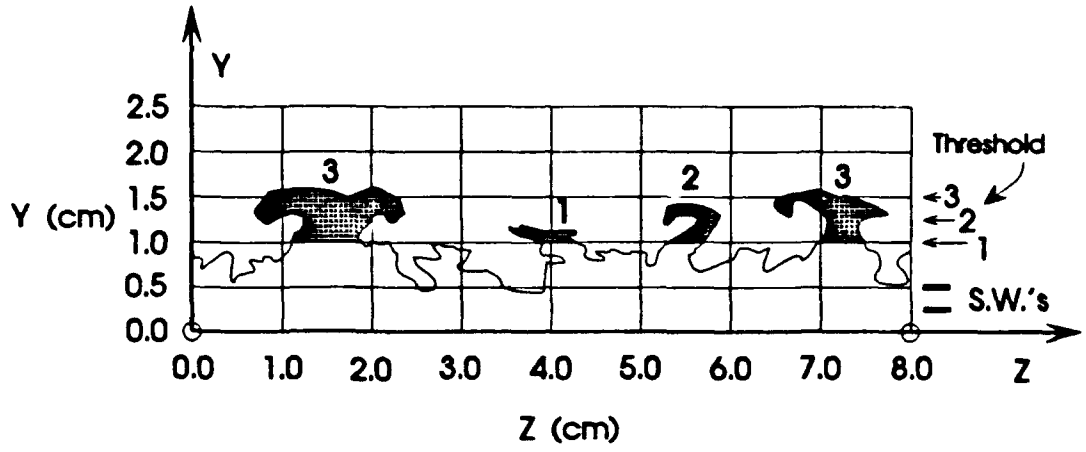

Figure 9a. Typical Trace Plot of a Low Smoke wire Z-Type Image.

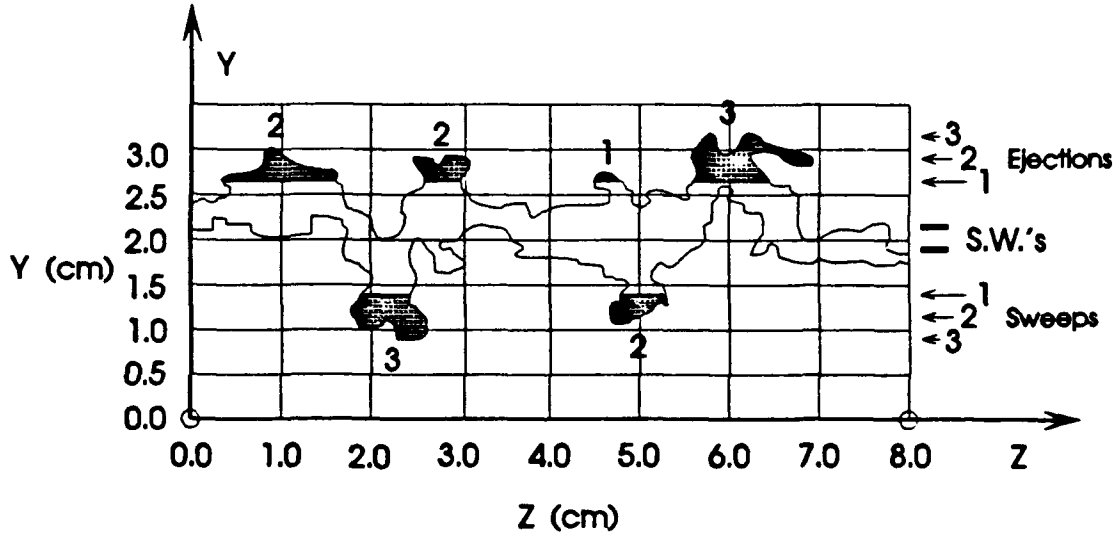

Figure 9b. Typical Trace Plot of a High Smoke Wire Z-Type Image.

of time. Figure 10 shows the probability- density histograms for the length of the structures. The plots indicate that the most probable duration of a structure is less than a $t^+ = 6$, and that the mean duration ranges between 18 t^+ and 22 t^+ for the various plain and undisturbed cases. If these structures are linked to counter rotating vortices lifting up the smoke in the middle of the structure, then these results would indicate that these vortices can be quite long, on the order of 900 x^+ (based on a convection speed of the mean velocity at a y^+ of 60), but are typically on the order of 300 x^+ units. This is in agreement with IIT's earlier experiments (Wark and Nagib, 1991, and Naguib and Wark, 1992) and with the direct numerical simulation data analyzed by Robinson (1991), where he found that typical legs trailing from hairpin-like vortices were on the order of 400 x^+ long.

The second facet of these events discussed is the spanwise spacing at which these events occur. Here the structures were identified using three different thresholds. For each threshold the structures were located in each frame and the spacing between two adjacent structures was calculated for every structure pair of that threshold in a film. The resulting statistics for the spacings are listed in Table 1, and some of them are plotted in Figure 11. The results indicate that the two plain cases show good repeatability including the standard deviation.

These dynamically-active structures have been identified to have normal velocities from 6 to 18 % of the local men velocity and to reach elevations well above 200 y^+ for the present Re_θ of 2080. The mean transverse spacing of these vertical structures is proportional to the height at which they are identified, with the more energetic structures more widely separated. The higher the elevation these structures are marked the wider their mean spacing appears to be in wall units, although this increase does not seem to be linear. The probability density functions of the spacing of these structures is strongly supportive of the hierarchy of scales for these dynamically active events as discussed by Wark and Nagib (1991) and Naguib and Wark (1992).

The last two films were of the high smoke wire type where both sweep and ejection type events were examined. Here only threshold one and two were available due to the limited number of structures appearing in these films. The PDF's for the threshold one case of sweeps and ejections is shown in Figure 11. The results in the case of one film confirm the hypothesis that the ejection events coming from the wall are stronger and larger than the sweep events going down towards the wall.

In summary, a new technique was developed where the spanwise occurrence of dynamically active events is investigated. Several characteristics of these structures have been revealed through this type of procedure. Finally, the effects of the present form of artificial disturbances were found to be minimal, and it is difficult to speculate as to their relation to the ejection events, beyond statements made in the previous section.

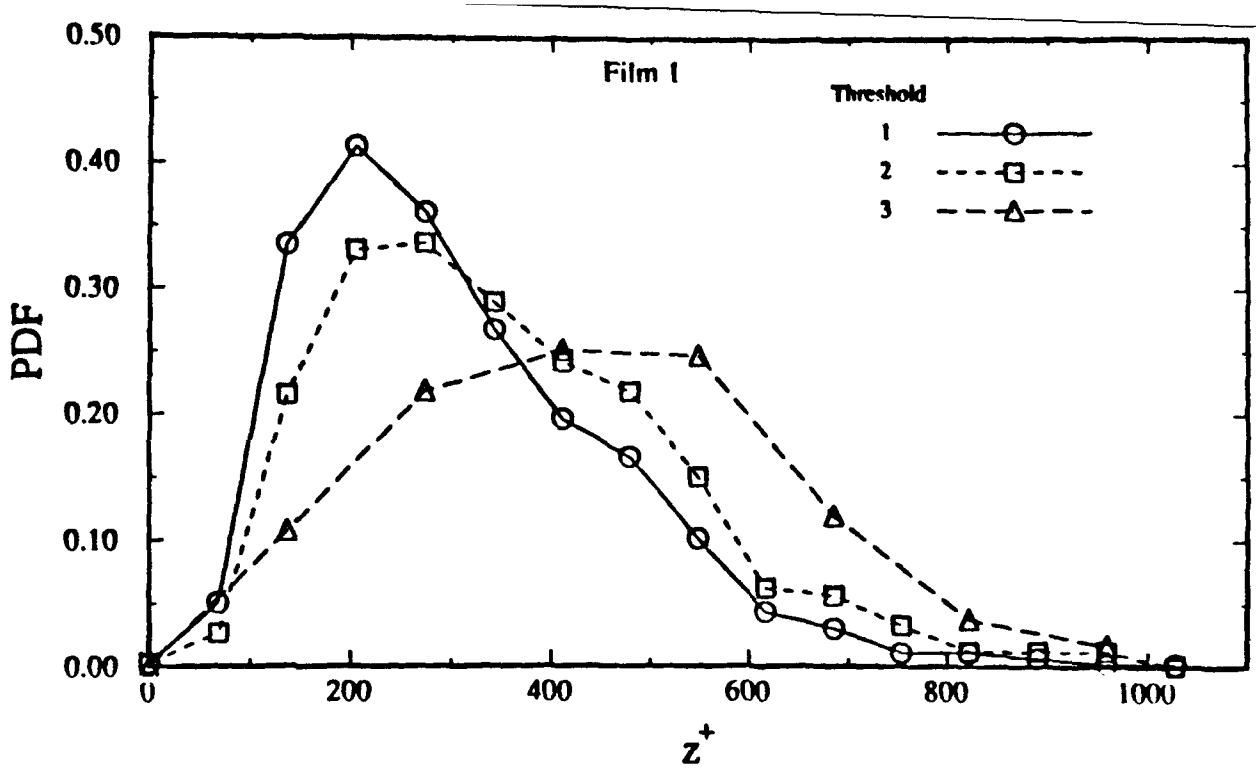

Figure 10. Comparison of PDF's of the Time-Duration of Structures from Film One (Plain Case) for Control Case and Three Tracking Thresholds.

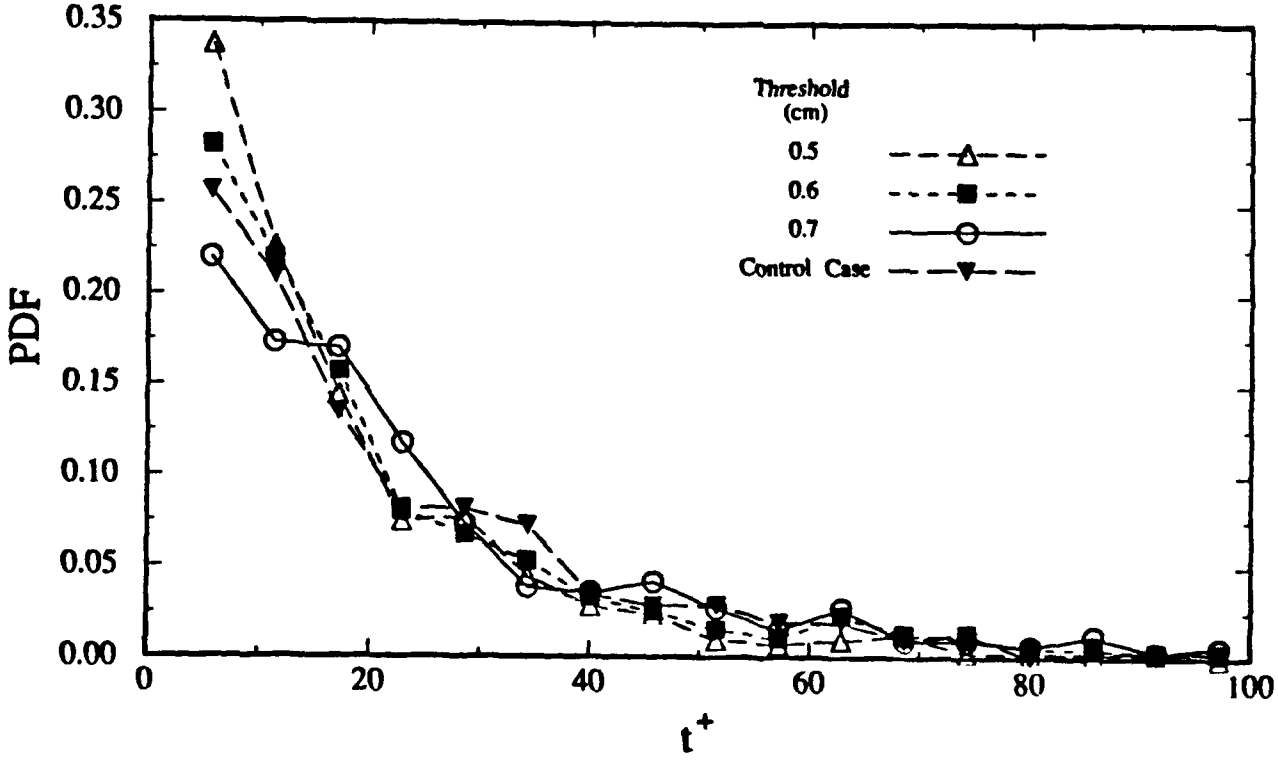

Figure 11. Threshold Effects on PDF's of Spanwise Spacing of Ejection Structures in Film One (Plain Case).

Table 1. Statistics of Spanwise Structure Spacing

Film:	Smoke wire heights (cm)	Thresh-hold	Number of structure pairs	Mean spacing λ^+	Std. dev. σ^+	Mean spacing λ^+ / dy^+	Mean spacing λ^+ / h^+
1: Control case	0.25,	1	926	308	155	4.50	2.25
(ejections)	0.50	2	678	354	170	3.44	2.08
		3	243	437	187	3.19	2.13
2: Control case	0.25,	1	854	315	152	4.60	2.30
(ejections)	0.50	2	490	371	174	3.61	2.17
		3	100	463	210	3.38	2.25
3: Bumps at	0.25,	1	615	343	174	5.00	2.50
$x^+ = 400$*	0.50	2	412	384	198	3.74	2.24
(ejections)		3	68	499	230	3.64	2.43
4: Bumps at	0.25,	1	609	341	161	4.98	2.49
$x^+ = 800$*	0.50	2	449	375	173	3.65	2.18
(ejections)		3	115	462	200	3.37	2.25
5: Ejections	1.90,	1	119	402	203	5.87	1.11
	2.15	2	43	456	203	4.43	1.15
Sweeps	1.90,	1	138	381	215	5.56	1.97
	2.15	2	48	378	199	3.71	2.40
6: Ejections	2.35,	1	79	370	235	5.40	0.87
	2.60	2	21	454	236	4.42	0.99
Sweeps	2.35,	1	296	336	184	4.91	1.75
	2.60	2	118	413	209	4.02	2.62

* Indicates the distance from the laser-light sheet to the row of bumps.

References

Adrian, R.J. 1991. *Particle-Imaging Techniques for Experimental Fluid Mechanics.* Annual Review of Fluid Mechanics, Vol. 23.

Antonia, R. A., Teitel M., Kim, J. and Browne, L. W. B. 1992. "Low-Reynolds-Number Effects in a Fully Developed Turbulent Channel Flow." *J. Fluid Mech.*, Vol. 236, pp. 579-605.

Antonia, R. A. and Bisset, D. K. 1990. *Spanwise Structure in the Near Wall Region of a Turbulent Boundary Layer.* J. Fluid Mech., Vol 210, pp. 437-458.

Blackwelder R.F. and Haritonidis, J.H. 1983. *Scaling of the bursting frequency in turbulent boundary layers.* J. Fluid Mech. Vol. 132, pp. 87-103

Blackwelder R.F. and Kovasznay L.S.G. 1972. *Time Scales and Correlations in a Turbulent Boundary Layer.* Physics of Fluids, Vol. 15, no. 9, pp. 1545-1554.

Corrsin S. and Kistler A.L. 1955. NACA Report no. 1244.

Guezennec, Y. G. 1985. *Documentation of Large Coherent Structures Associated With Wall Events in Turbulent Boundary Layers.* Ph.D. Thesis, Illinois Institute of Technology, Chicago, IL.

Guezennec, Y.G. and Nagib, H.N. 1990. *Mechanisms Leading to Net Drag Reductin in Manipulated Turbulent Boundary Layers.* AIAA Journal, Vol. 28, No. 2, pp. 245-252.

Hedley T.B. and Keffer J.F. 1974. *Turbulent/non-turbulent decisions in an intermittent flow.* J. Fluid Mech., Vol. 64, pp 625 - 644.

Kim, H.T., Kline, S.J. and Reynolds, W.C. 1971. *The production of turbulence near a smooth wall in a turbulent boundary layer.* J. Fluid Mech., Vol. 50, pp. 133-160.

Kovasznay, L.S.G., Kibens, V. and Blackwelder, R.F. 1970. *Large-scale motion in the intermittent region of a turbulent boundary layer.* J. Fluid Mech., Vol. 41, pp. 283.

Lekakis, I.C. 1988. *Coherent Structures in Fully Developed Turbulent Pipe Flow.* Ph.D. thesis, TAM Dept. University of Illinois at Urbana-Champaign.

Lu, S.S. and Willmarth, W.W. 1973. *Measurements of the Structure of the Reynolds Stress in a Turbulent Boundary Layer.* J. Fluid Mech., Vol. 60, pp. 481-511.

Luchik, T.S. and Tiederman, W.G. 1987. *Timescale and structure of ejections and bursts in turbulent channel flows.* J. Fluid Mech., Vol. 174, pp. 529-552.

McLean I.R. 1990. Ph.D. Thesis, University of Southern Cal., Los Angeles, CA

Naguib, A.M. and Wark, C.E. 1992. *Reynolds Number Effect on the Scales of Coherent Structures in a Turbulent Boundary Layer.* Submitted to Experiments in Fluids. Also M.S. thesis, A.M. Naguib, Illinois Institute of Technology.

Perry, A. E. and Abell, C. J. 1977. "Asymptotic Similarity of Turbulence Structures in Smooth- and Rough-Walled Pipes." *J. Fluid Mech.*, Vol. 79, 785-799.

Perry, A. E., Henbest, S. and Chong, M. S. 1986. "A Theoretical and Experimental Study of Wall Turbulence." *J. Fluid Mech.*, Vol. 165, 163-199.

Robinson, S.K. 1991. *The Kinematics of Turbulent Boundary Layer Structure.* NASA Technical Memorandum 103859, April 1991. Also Annual Review of Fluids, 1991. Also Ph.D. Thesis, Stanford University, 1990.

Spalart, P. R. 1988. *Direct Simulation of a Turbulent Boundary Layer Up to a* $Re_\theta = 1410$. J. Fluid Mech., Vol. 187, pp. 61-98.

Theodorsen, T. 1952. *Mechanism of Turbulence*. Proceedings Second Midwestern Conference on Fluid Mechanics, Bulletin No. 149. Ohio State University, Columbus, Ohio.

Wark, C. E. 1988. *Experimental Investigation of Coherent Structures in Turbulent Boundary Layers.* Ph. D. Thesis, Illinois Institute of Technology, Chicago, IL.

Wark, C.E., Hur, S.W. and Naguib, A.M. 1990. *Effects of Transition on the Reynolds-Stress Producing Events in a Turbulent Boundary layer.* Presented at the 28th Aerospace Sciences Meeting, January 8-11, 1990, Reno Nevada. Paper no. AIAA-90-0497.

Wark, C.E. & Nagib, H.M. 1991. *Experimental investigation of coherent structures in turbulent boundary layers.* J. Fluid Mech. Vol. 230, pp. 183-208.

Wark, C.E., Naguib, A.M. and Robinson, S.K. 1991. *Scaling of Spanwise Length Scales in a Turbulent Boundary Layer..* Presented at the 29th Aerospace Sciences Meeting, January 7-10, 1991, Reno Nevada. Paper no. AIAA-91-0235.

List of Publications, Theses and Presentations

Publications

Inner- and Outer-Layer Effects on the Dynamics of a Turbulent Boundary Layer. A.M. Naguib and C.E. Wark. To be submitted to **J. Fluid Mech.**

Characterization of Dynamically Active Events in Turbulent Boundary Layers. H.M. Nagib, D.W. Hathway, A.M. Naguib and C.E. Wark. **Proceedings of the International Conference on Near-Wall Turbulent Flows,** Tempe, Arizona, March 1993, Elsevier Science Publishers.

An Investigation of Wall-Layer Dynamics Using a Combined Temporal Filtering and Correlation Technique, A.M. Naguib and C.E. Wark. **J. Fluid Mech.,** Vol. 243, pp. 541-560.

Experimental Investigation of Coherent Structures in Turbulent Boundary Layers. C.E. Wark and H.M. Nagib. **J. Fluid Mech.**, Vol. 230, pp. 183-208.

Structure of Turbulence Using PIV in a Wall-Bounded Shear Flow, C.E. Wark, P.W. Offutt and R.J. Adrian. To be submitted to **Physics of Fluids**. Also presented as an invited lecture **at the 22nd Midwestern Mechanics Conference**, 6-9 October, 1991.

Theses

Inner- and Outer-Layer Effects on the Dynamics of a Turbulent Boundary Layer, A.M. Naguib, **Ph.D. thesis**, Illinois Institute of Technology, December 1992. Advised by C.E. Wark

Effects of Transition and Outer-Layer Intermittency on the Reynolds-Stress Producing Events in a Turbulent Boundary Layer, S.W. Hur, **M.S. thesis**, Illinois Institute of Technology, December 1991. Advised by C.E. Wark

Visualization of Dynamically Active Events in a Turbulent Boundary Layer, D.W. Hathway, **M.S. thesis**, Illinois Institute of Technology, December, 1991. Advised by H.M. Nagib

Presentations

Reynolds Number Effect on Coherent Structures in a Turbulent Boundary Layer. A.M. Naguib, C.E. Wark, S.K. Robinson and P.R. Spalart. **43rd Annual Meeting, Division of Fluid Dynamics of the American Physical Society**, Cornell University, 18-20 November 1990.

Structure of Turbulence Using PIV in Wall-Bounded Shear Flow. C.E. Wark, P.W. Offutt and R.J. Adrian. **43rd Annual Meeting, Division of Fluid Dynamics of the American Physical Society**, Cornell University, 18-20 November 1990.

Three-Dimensional Composite Images of Reynolds-stress Production Events in a Boundary Layer. D. Hathway and H.M. Nagib. **43rd Annual Meeting, Division of Fluid Dynamics of the American Physical Society**, Cornell University, 18-20 November 1990.

Relative Role and Interaction of Inner and Outer Layer Structures in the Near-Wall Region. A.M. Naguib and C.E. Wark, **44th Annual Meeting, Division of Fluid Dynamics of the American Physical Society**, Arizona State University, 24-26 November 1991.

Inner- and Outer-Layer Effects on the Dynamics of a Turbulent Boundary Layer. A.M. Naguib and C.E. Wark, **45th Annual Meeting, Division of Fluid Dynamics of the American Physical Society**, Florida State Univeristy, 22-24 November 1992.

Inner- and Outer-Layer Decomposition of Wall Layer Events in Turbulent Boundary Layers. H.M. Nagib, M.H. Hites and C.E. Wark. **46th Annual Meeting, Division of Fluid Dynamics of the American Physical Society**, University of New Mexico, 21-23 November 1993.

PIV Investigation of the Logarithmic Layer in a Turbulent Pipe Flow. C.E. Wark, P.W. Offutt and R.J. Adrian, **46th Annual Meeting, Division of Fluid Dynamics of the American Physical Society**, University of New Mexico, 21-23 November 1993.

Appendix

Reprints of Publications:

Experimental investigation of coherent structures in turbulent boundary layers. C.E. Wark and H.M. Nagib. **J. Fluid Mech.**, Vol. 230, pp. 183-208

An Investigation of Wall-Layer Dynamics Using a Combined Temporal Filtering and Correlation Technique, A.M. Naguib and C.E. Wark. **J. Fluid Mech.**, Vol. 243, pp. 541-560.

Characterization of Dynamically Active Events in Turbulent Boundary Layers. H.M. Nagib, D.W. Hathway, A.M. Naguib and C.E. Wark. **Proceedings of the International Conference on Near-Wall Turbulent Flows**, Tempe, Arizona, March 1993, Elsevier Science Publishers.

The following two publications are in preparation and will be forwarded upon completion.

Inner- and Outer-Layer Effects on the Dynamics of a Turbulent Boundary Layer. A.M. Naguib and C.E. Wark. To be submitted to **J. Fluid Mech.**

Structure of Turbulence Using PIV in a Wall-Bounded Shear Flow, C.E. Wark, P.W. Offutt and R.J. Adrian. To be submitted to **Physics of Fluids**.